

Image Matching across Wide Baselines: From Paper to Practice

Yuhe Jin¹ Dmytro Mishkin² Anastasiia Mishchuk³
 Jiří Matas² Pascal Fua³ Kwang Moo Yi¹ Eduard Trulls⁴

¹University of Victoria ²Czech Technical University in Prague ³École Polytechnique Fédérale de Lausanne ⁴Google Research

Abstract

We introduce a comprehensive benchmark for local features and robust estimation algorithms, focusing on the downstream task – the accuracy of the reconstructed camera pose – as our primary metric. Our pipeline’s modular structure allows us to easily integrate, configure, and combine methods and heuristics. We demonstrate this by embedding dozens of popular algorithms and evaluating them, from seminal works to the cutting edge of machine learning research. We show that with proper settings, classical solutions may still outperform the perceived state of the art.

Besides establishing the actual state of the art, the experiments conducted in this paper reveal unexpected properties of SfM pipelines that can be exploited to help improve their performance, for both algorithmic and learned methods. Data and code are online¹, providing an easy-to-use and flexible framework for the benchmarking of local feature and robust estimation methods, both alongside and against top-performing methods. This work provides the basis for an open challenge on wide-baseline image matching².

1. Introduction

Matching two or more views of a given scene is at the core of fundamental computer vision problems, including image retrieval [48, 7, 69, 91, 63], 3D reconstruction [3, 43, 79, 106], re-localization [74, 75, 51], and SLAM [61, 30, 31]. Despite decades of research, it remains unsolved in the general, wide-baseline scenario, as the number of factors to deal with can be exceedingly large: viewpoint, scale, rotation, illumination, occlusions, and camera properties render the problem very challenging in combination. Because of this, it has traditionally been approached with sparse methods – that is, with local features.

Recent efforts have moved towards end-to-end solutions [45, 10, 22], but they do not yet outperform classical methods [77, 105] that break the problem into separate steps. For example, in stereo one may extract local features, such

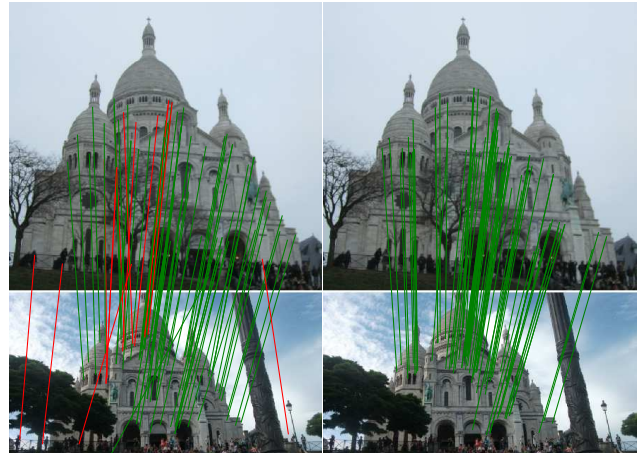


Figure 1. Every paper claims to outperform the state of the art. Is this possible, or an artifact of insufficient validation? On the left, we show stereo matches obtained with **D2-Net** (2019) [33], a state-of-the-art local feature, using OpenCV RANSAC with its default settings. On the right, we show **SIFT** (1999) [48] with a carefully tuned MAGSAC [29] – notice how the latter performs much better. We fill this gap with a new, modular benchmark for sparse image matching, with dozens of built-in methods.

as SIFT [48], build a list of putative matches by a nearest-neighbour search in descriptor space, and retrieve the pose with a minimal solver inside a robust estimator, such as the 7-point algorithm [41] in a RANSAC loop [36]. To build a 3D reconstruction out of a set of images, we would feed the same matches to a bundle adjustment pipeline [40, 93] to jointly optimize the camera intrinsics, extrinsics, and 3D point locations. This modular structure simplifies the problem and allows for incremental improvements, of which there have been hundreds, if not thousands.

New methods for each of these sub-problems, such as feature extraction or pose estimation, are typically studied in isolation, using intermediate metrics, which simplifies their evaluation. However, there is no guarantee that gains in one part of the pipeline will translate to the final application, as these components interact in complex ways. For example, patch descriptors, including very recent works [42, 97, 90, 60], are often evaluated on Brown’s seminal patch retrieval database [20], showing dramatic im-

¹<https://github.com/vcg-uvic/image-matching-benchmark>

²<https://vision.uvic.ca/image-matching-challenge>

improvements over handcrafted methods such as SIFT, but it is unclear whether this is also true on real-world applications – in fact, we later demonstrate that the gap may narrow dramatically when baselines are properly tuned.

We posit that it is time to look beyond intermediate metrics and focus on downstream performance. This is particularly crucial *now*, with deep networks seemingly outperforming algorithmic solutions on classical problems such as outlier filtering [100, 70, 102, 85, 18], bundle adjustment [86, 81], SfM [96, 5] and SLAM [87, 46]. To this end, we introduce a benchmark for wide-baseline image matching, including: (a) A dataset with 30k images with depth maps and ground truth poses (called posed images later). (b) A modular pipeline incorporating dozens of methods for feature extraction and matching, and pose estimation, both classical and state-of-the-art, as well as multiple heuristics, which can be swapped out and tuned separately. (c) Two downstream tasks – stereo and multi-view reconstruction – evaluated with downstream and intermediate metrics. (d) A thorough study of dozens of methods and techniques, hand-crafted and learned, and their combination, along with a procedure for hyper-parameter selection.

This framework will enable researchers to evaluate how a new approach performs in a standardized pipeline, both *against* its competitors, and *alongside* state-of-the-art solutions for other components, from which it cannot be truly detached. This is crucial, as true performance can be easily hidden by sub-optimal hyperparameters. Data and code are publicly available.

2. Related Work

The literature on image matching is too vast for a thorough overview. We cover relevant methods for feature extraction and matching, pose estimation, 3D reconstruction, datasets, and evaluation frameworks.

Local features. Local features became a staple in computer vision with the introduction of SIFT [48]. They typically involve three distinct steps: keypoint detection, orientation estimation, and descriptor extraction. Other popular, hand-crafted solutions are SURF [15], ORB [73], and AKAZE [4]. Modern descriptors train deep networks on pre-cropped patches, typically from SIFT keypoints (*i.e.* Difference of Gaussians or DoG). They include Deepdesc [82], TFeat [11], L2-Net [89], Hardnet [57], SOS-Net [90], and LogPolarDesc [34] – most of them are trained on the same dataset [20]. Recent work leverage additional cues, such as geometry or global context, including GeoDesc [50] and ContextDesc [49]. There have been multiple attempts to learn keypoint detectors separately from the descriptor, including TILDE [95], TCDet [103], QuadNet [78], and KeyNet [13]. An alternative is to treat this as an end-to-end learning problem, a trend that started with

the introduction of LIFT [99] and also includes DELF [63], SuperPoint [31], LF-Net [64], D2-Net [33] and R2D2 [72].

Robust matching. Inlier ratios in wide-baseline stereo can be below 10% – and sometimes much lower. This is typically approached with iterative sampling schemes based on RANSAC [36], relying on closed-form solutions for pose solving such as the 5- [62], 7- [41] or 8-point algorithm [39]. Improvements to this classical framework include local optimization [24], MLESAC [92], PROSAC [23], DEGENSAC [26], GC-RANSAC [12], and MAGSAC [29]. Recent efforts, starting with CNe (Context Networks) in [100], train deep networks for outlier rejection taking correspondences as input, often followed by a RANSAC loop. Follow-up works include [70, 104, 85, 102]. Despite their promise, it remains unclear how well they perform in real settings.

Structure from Motion. In Structure-from-Motion (SfM) one jointly optimizes the location of the 3D points and the camera intrinsics and extrinsics. Many improvements have been proposed over the years [3, 43, 27, 37, 106]. The most popular frameworks are VisualSfM [98] and COLMAP [79] – we rely on the latter, to generate the ground truth and as the backbone of our multi-view task.

Datasets and benchmarks. Early work relied on the Oxford dataset [54], with 48 images and ground truth homographies. It helped establish two common metrics: repeatability and matching score. Repeatability evaluates the keypoint detector – given keypoint sets over two images, projected into each other, it is defined as the ratio of keypoints whose support region overlap is above a threshold. The matching score (MS) is similarly defined, but also requires their descriptors to be nearest neighbours. Both require pixel-to-pixel correspondences – features outside valid areas are ignored. A modern alternative to Oxford is HPatches [9], which contains 696 images with differences in illumination *or* viewpoint – the scenes are planar, without occlusions. Other datasets include DTU [1], Edge Foci [107], Webcam [95], AMOS [67], and Strecha’s [83]. They all have limitations – narrow baselines, noisy ground truth, or contain few images. Learned descriptors are often trained and evaluated on [21], where they outperform SIFT by orders of magnitude – probably due to overfitting. Datasets used for navigation, re-localization or SLAM in outdoor environments are also relevant, including Kitty [38], Aachen [76], Robotcar [52], and CMU seasons [75, 8], but may not feature the wide range of transformations present in Phototourism data. This includes Megadepth [47], a dataset which builds on COLMAP – and could be folded into ours.

Modern benchmarks, by contrast, are few and far between – they include VLBenchmark [44], HPatches [9], and SILDa [35] – all limited in scope. A large-scale benchmark for SfM was proposed in [80] – without ground truth. A recent work by Bian *et al.* [17] evaluates different methods for



Figure 2. **Phototourism dataset.** Some images in our dataset and their corresponding depth maps, with occlusions shown in red.

pose estimation on several datasets – however, few methods are considered and they are not carefully tuned. We are, to the best of our knowledge, the first to introduce a public, comprehensive, and modular benchmark for sparse methods with downstream metrics.

3. The Phototourism Dataset

A wide range of imaging conditions and devices is necessary in order to compile a strong dataset – Phototourism images fit this description and are readily available. We thus build on 26 collections of popular landmarks originally selected in [43, 88], each with hundreds to thousands of images. We downsample them to a maximum size of 1024 pixels and pose them with COLMAP [79]. In addition to point clouds, COLMAP provides noisy but dense depth estimates. We remove occlusions from them using the reconstructed model: see Fig. 2 for examples. We rely on these depth maps to compute pixel-wise metrics – repeatability and matching score. We find that some images are flipped 90°, and use the poses to rotate them so they are roughly ‘upright’. We select 2 scenes for validation, 11 for testing, and the rest for training – see the appendix for details.

Our core assumption is that we can obtain ‘accurate’ poses from large sets of images, which we then use as ‘ground truth’ to evaluate image matching on pairs or small subsets of images – a harder, proxy task. The improvement in accuracy with more images can be measured by incrementally adding images into a reconstruction, picking a fixed set of image pairs, present in all reconstructions, and computing their relative pose change – analogously to how we compute errors in the benchmark. In ‘Sacre Coeur’ set, increasing the number of images from 25→50 results in a median pose difference (maximum of ΔR and ΔT) of 0.57°. At 50→100 this becomes 0.21°, and for 100→200 and after it stabilizes to 0.07-0.09°. This is much smaller than the first bin size in our evaluation metric (1°), which we intentionally set to account for noise in the ground truth.

After reconstructing the scene, we select $N=100$ images for each test scene – which keeps feature extraction and matching tractable.

For the stereo task, we sub-sample co-visible pairs of images with a simple heuristic: we extract, for each im-

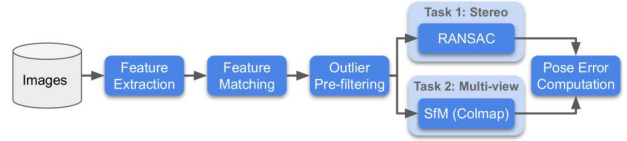


Figure 3. **The benchmark pipeline** takes N images of a scene as input, extracts features for each, and computes matches for all M image pairs, $M = \frac{1}{2}N(N-1)$. After an optional filtering step, the matches are fed to two different tasks. Performance is measured *downstream*, by a pose-based metric, common across tasks.

age, the 2D keypoints present in the 3D model, obtain their bounding box, and compute the ratio between its area and the whole image. Given a pair of images, we pick the minimum of the two as the ‘co-visibility’ ratio $v_{i,j} \in [0, 1]$. It varies from scene to scene – we histogram it in the appendix. For the multi-view task, we simply select image subsets which have at least 100 3D points in common, as in [100, 102]. We find both criteria work well in practice.

4. Pipeline

Our pipeline is outlined in Fig. 3. It takes as input $N=100$ images per scene. The feature extraction module computes up to K features from each image. The feature matching module generates a list of putative matches for each image pair, *i.e.* $\frac{1}{2}N(N-1) = 4950$ combinations. These matches can be optionally processed by an outlier pre-filtering module. They are then fed to two tasks: stereo, and multi-view reconstruction with SfM. We now describe each of these components in detail.

Feature extraction. We consider three broad families of local features. The first includes full, hand-crafted pipelines: SIFT [48] (and RootSIFT [6]), SURF [15], ORB [73], and AKAZE [4]. We take these from OpenCV. For all of them, except ORB, we lower the detection threshold to extract more features, which increases performance. We also consider DoG alternatives from VLFeat [94]: (VL-)DoG, Hessian [16], Hessian-Laplace [55], Harris-Laplace [55], MSER [53]; and their affine-covariant versions: DoG-Affine, Hessian-Affine [55, 14], DoG-AffNet [59], and Hessian-AffNet [59]. The second group includes descriptors learned on DoG keypoints: L2-Net [89], Hardnet [57], Geodesic [50], SOSNet [90], ContextDesc [49], and LogPolarDesc [34]. The last group consists of pipelines learned end-to-end (e2e): Superpoint [31], LF-Net [64], and D2-Net [33] – the latter with single- (SS) and multi-scale (MS) variants. Finally, we consider Key.Net [13], a learned detector paired with HardNet descriptors – their implementation performs poorly for us so we pair it with our own HardNet.

Feature matching. We break this step into four stages. Given images \mathbf{I}^i and \mathbf{I}^j , $i \neq j$, we create an initial set of matches by nearest neighbor (NN) matching from \mathbf{I}^i to \mathbf{I}^j ,

obtaining a set of matches $\mathbf{m}_{i \rightarrow j}$. We optionally do the same in the opposite direction, $\mathbf{m}_{j \rightarrow i}$. We then apply Lowe’s ratio test [48] to each list to filter out non-discriminative matches, with a threshold $r \in [0, 1]$, creating ‘curated’ lists $\tilde{\mathbf{m}}_{i \rightarrow j}$ and $\tilde{\mathbf{m}}_{j \rightarrow i}$. We obtain the final set of putative matches by taking their intersection, $\tilde{\mathbf{m}}_{i \rightarrow j} \cap \tilde{\mathbf{m}}_{j \rightarrow i} = \tilde{\mathbf{m}}_{i \leftrightarrow j}^\cap$ (known in the literature as one-to-one, mutual NN, bipartite, or cycle-consistent), or their union $\tilde{\mathbf{m}}_{i \rightarrow j} \cup \tilde{\mathbf{m}}_{j \rightarrow i} = \tilde{\mathbf{m}}_{i \leftrightarrow j}^\cup$ (symmetric). We refer to them as ‘both’ and ‘either’ respectively. We also implement simple unidirectional matching, *i.e.*, $\tilde{\mathbf{m}}_{i \rightarrow j}$. Finally, we optionally apply a distance filter, removing matches whose distance is above a threshold.

Outlier pre-filtering. Context Networks [100], or CNe, proposed a method to find sparse correspondences with a permutation-equivariant deep network based on PointNet [68], and sparked a number of follow-up works [70, 28, 104, 102, 85]. We embed CNe into our framework. It works best paired with RANSAC [100, 85], so we consider it as an *optional* pre-filtering step – for both stereo and multi-view. As their published model was trained on one of our validation scenes, we re-train it on ‘Notre Dame’ and ‘Buckingham Palace’, following their training protocol, with 2000 SIFT features, unidirectional matching, and no ratio test.

Stereo task. The list of putative matches is given to a robust estimator, which we use to estimate $\mathbf{F}_{i,j}$, the Fundamental matrix between \mathbf{I}_i and \mathbf{I}_j . In addition to (locally-optimized) RANSAC [36, 25], as implemented in OpenCV [19] and sklearn [65], we consider recent algorithms: DEGENSAC [26], GC-RANSAC [12] and MAGSAC [29]. For DEGENSAC we additionally consider disabling the degeneracy check, which theoretically would be equivalent to the OpenCV and sklearn implementations – we call this variant ‘PyRANSAC’. Given $\mathbf{F}_{i,j}$, we use the known intrinsics $\mathbf{K}_{\{i,j\}}$ to compute the Essential matrix $\mathbf{E}_{i,j}$, as $\mathbf{E}_{i,j} = \mathbf{K}_j^T \mathbf{F}_{i,j} \mathbf{K}_i$. Finally, we recover the relative rotation and translation vectors with a cheirality check with OpenCV’s `recoverPose`.

Multi-view task. Large-scale SfM is notoriously hard to evaluate, as it requires accurate ground truth. Since our goal is to benchmark *local features*, not SfM itself, we opt for a different strategy. In this task we reconstruct a scene from small image subsets, which we call ‘bags’. We consider bags of 3, 5, 10, and 25 images, which are randomly sampled from the original set of 100 images per scene, with a co-visibility check. We create 100 bags for bag sizes 3 and 5, 50 for bag size 10, and 25 for bag size 25 – 275 SfM runs in total. We use COLMAP [79], feeding it the matches computed by the previous module – note that this comes before the robust estimation step, as COLMAP implements its own RANSAC. If multiple reconstructions are obtained, we consider the largest one. We also collect statistics such as the number of landmarks or the average track length. Both

statistics and error metrics are averaged over the four bag sizes, each of which is in turn averaged over its bags.

Error metrics. We compute the angular error between the estimated and ground-truth translation and rotation vectors between two cameras, threshold over a given value, and compute the mean Average Precision (mAP) by integrating the curve up to that threshold – we find 10° adequate. We also use this metric for multi-view, as the scenes are not up to scale and it is not possible to measure translation error in metric terms (we will explore this in the future). To do so, we average the error every pair of cameras (setting it to ∞ for unregistered views). For stereo, we can report this value for different co-visibility thresholds: we use $v = 0.1$, which preserves ‘hard’ pairs. Finally, we consider repeatability and matching score – as end-to-end methods do not report scale, we threshold by pixel distance. We also compute the Absolute trajectory error (ATE) [84], a metric widely used in SLAM, for our multiview task. As, again, the reconstructed model is without scale, we first scale the reconstructed model to the scale of the ground truth and then compute ATE. It needs a minimum of three points to align the two models – we only compute it for reconstructions with at least three registered images.

Implementation. Code is open-sourced, along with every method used in the paper³. Our implementation relies on Slurm for job scheduling – we will provide on-the-cloud, ready-to-go images. It can also run on a standard computer, sequentially. It is computationally expensive, as it requires matching over 50k image pairs. The most costly step is feature matching: 2-6 s. per image pair, depending on descriptor size. Outlier pre-filtering takes about 0.5-0.8 s. per pair, overhead aside. RANSAC methods vary between 0.5-1 s. – as explained in Section 5 we limit their number of iterations based on a compute budget, but the actual cost depends on the number of matches. We find COLMAP to vary drastically between set-ups. New methods will be continuously added, with contributions welcome.

5. Details are Important

Our experiments indicate that each method needs to be carefully tuned. In this section we outline the methodology we used to find the right hyperparameters on the validation set, and demonstrate why it is crucial to do so.

RANSAC: Leveling the field. Robust estimators are the most sensitive part of the stereo pipeline. All methods have three parameters in common: the confidence level in their estimates, τ ; the outlier epipolar threshold, η ; and the maximum number of iterations, Γ . The confidence value is the least sensitive, so we set it to $\tau = 0.999999$. We evaluated

³<https://github.com/vcg-uvic/image-matching-benchmark-baselines>

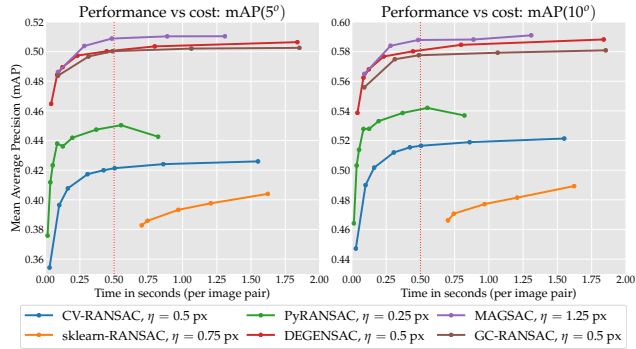


Figure 4. **RANSAC – Performance vs. cost.** We evaluate six RANSAC variants, using 8k SIFT features with ‘both’ matching and ratio test $r=0.8$. The inlier threshold η and iterations limit Γ are variables – we plot only the best η for each method, for clarity, and set a budget of 0.5s. (dotted red line). Computed on ‘n1-standard-2’ VMs on Google Compute (2 vCPUs, 7.5 GB).

each method for different Γ and η pictured in Fig. 5, along with their computational cost in Fig. 4. We place all methods on an ‘even ground’ by setting a common budget of 0.5 seconds, where all methods have mostly converged – we do so by choosing Γ as per Fig. 4, instead of actually enforcing a time limit. Optimal values for Γ can vary drastically, from 10k for MAGSAC to 250k for PyRANSAC. The best results are obtained by MAGSAC, followed by DEGENSAC. We patch OpenCV to increase the limit of iterations, which is hardcoded to $\Gamma = 1000$. This increases performance by 10-15% relative, within our budget. However, PyRANSAC is better, so we use it as our ‘vanilla’ RANSAC instead. The sklearn implementation is too slow for practical use.

We find that, in general, default settings can be woefully inadequate. For example, OpenCV sets $\tau = 0.99$ and $\eta = 3$ pixels, which results in a mAP at 10° of 0.5292 on the validation set – a performance drop of 23.9% relative.

RANSAC: One method at a time. The last free parameter is the inlier threshold η . We expect the optimal value for this parameter to be different for each local feature, with looser thresholds required for methods operating on higher recall/lower precision. We report a wide array of experiments in Fig. 5, which confirm our intuition: descriptors learned on DoG keypoints are clustered, while others vary significantly. Optimal values are also different for each RANSAC variant. We use the ratio test with recommended values for each feature (or a reasonable value if no recommendation exists), as there are too many outliers otherwise.

Ratio test: One feature at a time. Having set RANSAC, we turn to the feature matcher. Bidirectional matching with the ‘both’ strategy – the one we used so far – performs best overall. Unidirectional matching is slightly worse, and depends on the order of the images. Bidirectional matching with ‘either’ produces too many (false) matches, increasing

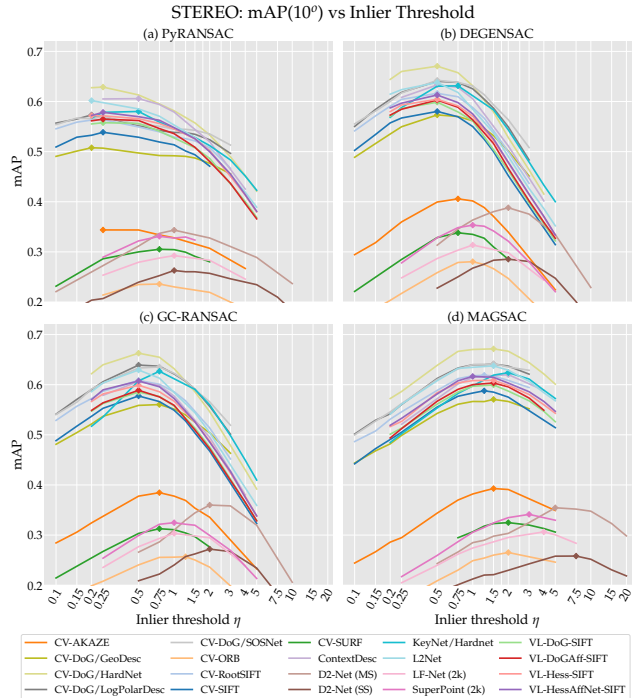


Figure 5. **RANSAC – Inlier threshold η .** We determine η for each combination, using 8k features with ‘both’ matching (2k for LF-Net and SuperPoint) with their recommended ratio test threshold. Optimal parameters (diamonds) are listed in the appendix.

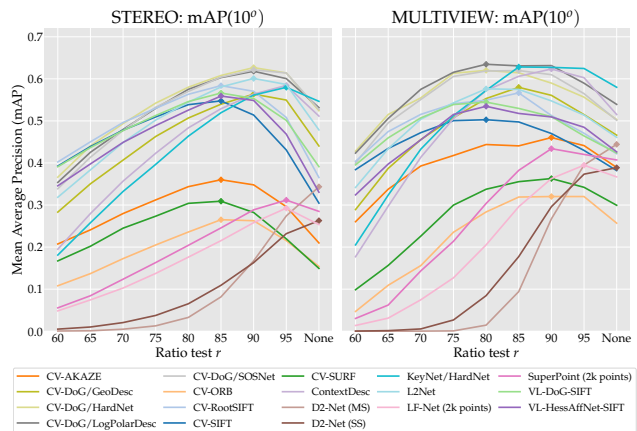


Figure 6. **Feature matching.** We evaluate bidirectional matching with the ‘both’ strategy (the optimal one), and different ratio test thresholds r , for each feature type. We use 8k features (2k for SuperPoint and LF-Net). For stereo, we use PyRANSAC.

the computational cost in the estimator, and requires very small ratio test thresholds – as low as $r=0.7$. We report these results in the appendix, and focus on the best strategy, *i.e.*, ‘both’. We select PyRANSAC as a ‘baseline’ RANSAC and evaluate different ratio test thresholds in Fig. 6.

As expected, each feature requires different settings, as the distribution of their descriptors is different. We also observe that optimal values vary significantly between stereo and multi-view, even though one would expect that bundle

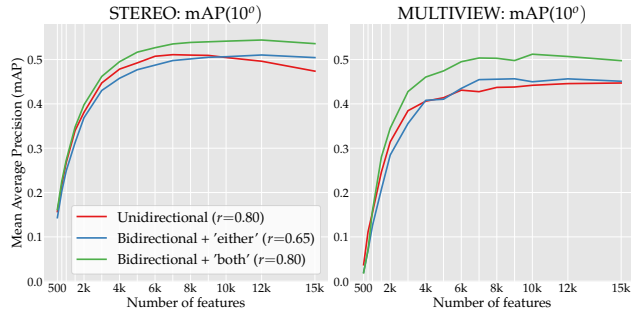


Figure 7. **Number of features.** Performance on stereo and multi-view, varying the number of SIFT features, with different matching strategies and recommended values for the ratio test r .

adjustment would be able to better deal with outliers. We suspect this might be due to potentially sub-optimal parameters on COLMAP’s RANSAC – we will evaluate this in the future. Interestingly, D2-Net is the *only* method which performs best without the ratio test. Note how the ratio test is critical for performance, and one could arbitrarily select a threshold that favours one method over another, which shows the importance of proper benchmarking.

Additionally, we implement the first-geometric-inconsistent ratio threshold, or FGINN [58], but find that although it improves over unidirectional matching, its gains disappears against matching with ‘both’ – see appendix.

Choosing the number of features. The ablation tests in this section use (up to) $K=8000$ features⁴, a number commensurate with that used by SfM frameworks [98, 79]. Fig. 7 evaluates different values for K . We use PyRANSAC with optimal settings, three matching strategies, and the recommended ratio test $r=0.8$ [48]. As expected, performance is strongly correlated with the number of features. We find 8k to be a good compromise between performance and cost, and also consider 2k (actually 2048) as a ‘cheaper’ alternative – this also provides a fair comparison with some learned methods which only operate on that regime.

Stereo mAP is higher than multi-view in Figs. 6-7. This might be surprising, as stereo is typically *harder* – this is due to how we compute it. First, we feed the multi-view task image subsets with looser co-visibility requirements. Second, every pair of images which contains one unregistered image is classified as a failure – and we consider only the largest reconstructed model, for simplicity, marking the images on smaller models as unregistered (this is rare).

Binary features. Binary descriptor papers favour a distance threshold in place of the ratio test to reject non-discriminative matches [73]. We evaluate both in Fig. 8. The ratio test works better for both ORB and AKAZE.

On the influence of the detector. We embed several

⁴2k for SuperPoint and LF-Net, as they are built for fewer keypoints.

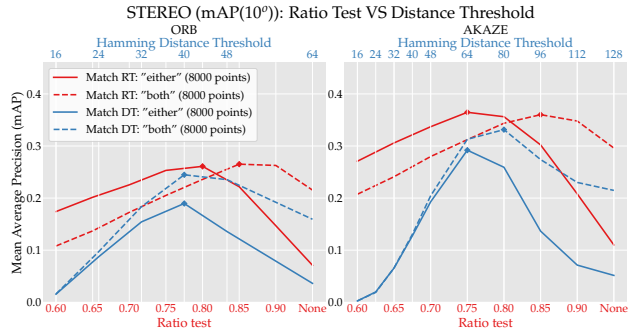


Figure 8. **Matching binary descriptors.** We filter out non-discriminative matches with the ratio test or a distance threshold. The latter (the standard) performs worse in our experiments.

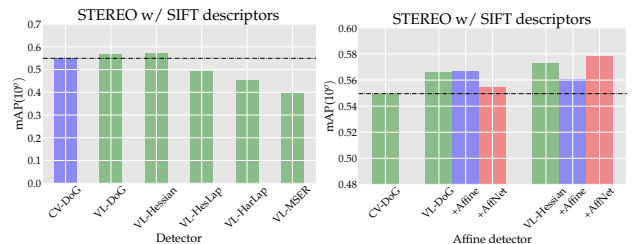


Figure 9. **Benchmarking detectors.** Performance on stereo, paired with SIFT descriptors. The dashed, black line indicates OpenCV SIFT. **Left:** OpenCV DoG vs. VLFeat implementation of blob detectors (DoG, Hessian, HesLap) and corner detectors (Harris, HarLap), and MSER. **Right:** affine shape estimation for DoG and Hessian keypoints, versus the plain version. We consider a classical approach, Baumberg (Affine) [14], and the recent, learned AffNet [59] – they provide a small but inconsistent boost.

popular blob and corner detectors into our pipeline, with OpenCV’s DoG [48] as a baseline. We combine multiple methods, taking advantage of the VLFeat library: DoG, Hessian [16], HessianLaplace [55], HarrisLaplace [55], MSER [53], DoGAffine, Hessian-Affine [55, 14], DoG-AffNet [59], and Hessian-AffNet [59]. We report results in Fig. 9, paired with SIFT descriptors. VLFeat’s DoG performs marginally better than OpenCV’s. Its affine version gives a small boost. Given the small gain and the infrastructure burden of interacting with a Matlab/C library, we use OpenCV’s DoG implementation for most of this paper.

On increasing the support region. The size (scale) of the support region used to compute a descriptor can significantly affect its performance [32, 101, 2]. We experiment with different scaling factors, using DoG with SIFT and HardNet [57], and find that 12x the OpenCV scale is already nearly optimal, confirming the findings in [34]; see the appendix for details.

6. Results on the Test Set

With the findings reported in Section 5, we move on to the test set, benchmarking many methods with their opti-

Method	PyRANSAC			DEGENSAC		MAGSAC		Rank
	NF	NI [†]	mAP(10°) [†]	NI [†]	mAP(10°) [†]	NI [†]	mAP(10°) [†]	
CV-SIFT	7879.0	153.9	.4160	222.7	.4608	270.6	.4586	13
VL-SIFT	7901.0	166.2	.4137	241.2	.4643	301.0	.4638	12
VL-Hessian-SIFT	8000.0	186.5	.3915	264.0	.4489	318.0	.4394	15
VL-DoGAff-SIFT	7910.9	218.6	.4049	229.7	.4653	291.9	.4624	11
VL-HesAffNet-SIFT	8000.0	190.8	.4081	271.6	.4659	328.5	.4581	10
CV-√SIFT	7884.0	176.3	.4348	257.4	.4921	317.4	.4891	6
SURF	7749.0	113.0	.2326	117.8	.2452	136.1	.2481	19
AKAZE	7879.8	184.3	.2738	232.7	.3142	284.4	.3054	17
ORB	7128.2	113.1	.1381	136.6	.1723	163.2	.1632	22
DoG-HardNet	7884.1	229.9	.4668	342.2	.5286	404.0	.5147	1
DoG-HardNetAmos+	7884.1	213.6	.4511	316.9	.5125	373.5	.5011	3
L2Net	7884.8	190.2	.4478	280.9	.4971	329.1	.4884	5
Key.Net-HardNet	7998.1	353.3	.3990	375.2	.4700	636.5	.4529	9
Geodesc	7884.3	179.7	.4183	264.0	.4787	340.3	.4753	8
ContextDesc	4811.1	248.8	.4283	261.4	.4856	356.1	.4662	7
SOSNet	7884.3	215.1	.4595	319.8	.5233	418.5	.5177	2
LogPolarDesc	7884.3	243.5	.4495	366.0	.5080	461.0	.5001	4
SuperPoint (2k)	1178.9	88.1	.2359	84.7	.2669	113.2	.2620	18
LF-Net (2k)	2024.8	95.1	.1945	100.8	.2253	134.2	.2164	20
D2-Net (SS)	5540.7	273.5	.1432	100.8	.1639	428.0	.1560	23
D2-Net (MS)	6806.3	193.8	.1690	322.8	.1836	505.1	.1731	21

Table 1. **Stereo – Test set.** We report: (NF) Number of Features; (NI) Number of Inliers produced by RANSAC; and mAP(10°). Top three methods by mAP marked in red, green and blue.

Method	NL [†]	SR [†]	RC [†]	TL [†]	mAP(5°) [†]	mAP(10°) [†]	ATE [‡]	Rank
CV-SIFT	2567.4	89.1	95.6	3.51	.3772	.4626	.7475	9
CV-√SIFT	2798.4	91.2	96.2	3.62	.4148	.5053	.6908	8
SURF	2421.7	84.5	93.9	3.11	.2591	.3353	.8259	13
AKAZE	3258.8	89.4	95.9	3.45	.3388	.4256	.7604	10
ORB	2341.1	84.5	92.1	3.09	.1905	.2529	.9165	16
DoG-HardNet	2834.1	91.5	96.3	3.79	.4644	.5599	.6669	1
L2Net	2413.7	88.0	95.2	3.70	.4383	.5308	.6656	6
Key.Net-HardNet	3755.3	96.6	98.0	3.89	.4438	.5456	.6688	4
Geodesc	2631.8	89.4	95.9	3.72	.4325	.5258	.6729	7
ContextDesc	2223.8	90.2	96.4	3.66	.4393	.5354	.6697	5
SOSNet	2681.6	90.1	96.4	3.81	.4650	.5592	.6583	2
LogPolarDesc	3029.7	90.1	95.6	3.79	.4622	.5565	.6657	3
SuperPoint (2k)	762.5	83.0	92.7	3.76	.2959	.3814	.7767	11
LF-Net (2k)	1014.6	80.0	89.8	3.63	.2936	.3723	.7517	12
D2-Net (SS)	3302.8	90.0	95.8	3.17	.2056	.2933	.8595	15
D2-Net (MS)	4022.9	93.7	97.0	3.05	.2143	.3149	.8335	14

Table 2. **Multiview – Test set.** We report: (NL) Number of 3D Landmarks; (SR) Success Rate (%) in the 3D reconstruction across ‘bags’; (RC) Ratio of Cameras (%) registered in a ‘bag’; (TL) Track Length or number of observations per landmark; mAP at 5-10°; and (ATE) Absolute Trajectory Error. All metrics are averaged across different ‘bag’ sizes, as explained in Section 4. We rank them by mAP at 10° and color-code them as in Table 1.

mal settings. All experiments in this section use bidirectional matching with the ‘both’ strategy. We provide multiple statistics and break down the results by scene. Qualitative results are available in the appendix.

The actual state of the art. We evaluate a large number of detector/descriptor combinations on the stereo task, paired with different RANSAC variants, with their optimal settings, and report the results in Table 1. We consider DEGENSAC and MAGSAC, which perform the best in the validation set, and PyRANSAC as a ‘baseline’ RANSAC. Deep descriptors on DoG keypoints are at the top, with HardNet being #1. Interestingly, ‘HardNetAmos+’ [56], a version trained on more datasets (Brown [20], HPatches [9] and AMOS [67]), performs worse than the original mod-

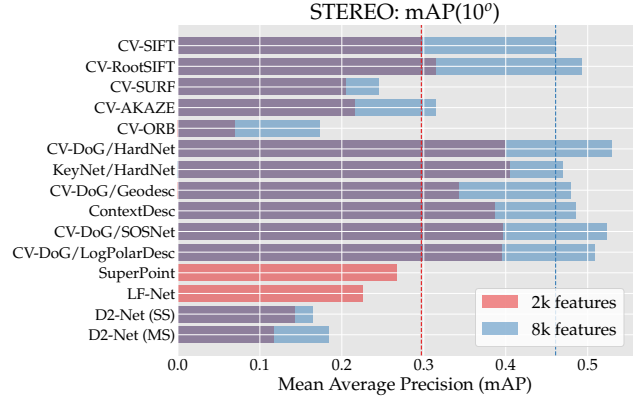


Figure 10. **Number of features – 2k vs 8k.** Performance on the test set, stereo task with DEGENSAC. Dashed lines indicate SIFT’s performance. We do not include results for 8k points with LF-Net, Superpoint, as we failed to obtain meaningful results.

els trained only on the ‘Liberty’ scene from Brown. Properly tuned, SIFT – RootSIFT specifically – performs within 7.4% relative of the state of the art. Other ‘classical’ local features do not fare so well. Key.Net produces more inliers than DoG, but its poses are slightly worse – note that these are the inliers *estimated* by each method, which may still contain outliers. D2-net performs poorly on our benchmark, despite state-of-the-art results on others – this might be related to its incompatibility with the ratio test, resulting in too many matches, and may require a different approach.

Table 2 reports results for the multi-view task. We see similar results, with deep descriptors operating on DoG points at the top, with HardNet first. Key.Net and D2-Net are able to reconstruct more views and produce more landmarks, with lower mAP. Interestingly, the rank may change between the tasks, with ORB performing better than single-scale D2-Net on stereo but significantly worse on multi-view, despite extracting 29% more features.

Performing on a budget. We also consider reducing the number of features from 8k to 2k, for the stereo task. This provides a fairer comparison with LF-Net and Superpoint, which we use with their recommended settings, as despite our best efforts we could not obtain meaningful results with 8k point, as they are not trained for it. We show the results in Fig. 10. The top performing methods do not change, but the gap with traditional features is wider. Interestingly, Key.Net outperforms DoG (paired with HardNet) and tops the chart – which makes sense, as it was trained for this regime.

Outlier pre-filtering with deep networks. Next, we study the performance of CNe [100] for outlier rejection. Its training data does not use the ratio test, so we omit it here too. Our initial experiments, with SIFT, are encouraging: CNe aggressively filters out about 80% of the matches in a single forward pass, boosting mAP at 10° by 3-5% relative on the stereo task across different RANSAC variants, despite pro-

Method	PyRANSAC		Stereo Task DEGENSAC		MAGSAC		Multi-view Task	
	mAP(10°) [†]	Δ(%) [†]	mAP(10°) [†]	Δ(%) [†]	mAP(10°) [†]	Δ(%) [†]	mAP(10°) [†]	Δ(%) [†]
CV-SIFT	.4260	+2.39	.4727	+2.58	.4735	+3.26	.4169	+10.52
CV-√SIFT	.4280	-1.55	.4867	-1.11	.4762	-2.63	.4317	+4.08
SURF	.2583	+11.05	.3086	+25.82	.3004	+21.09	.3466	+33.75
AKAZE	.3010	+9.92	.3539	+12.66	.3427	+12.22	.3738	+10.35
ORB	.1629	+17.94	.2067	+19.92	.1961	+20.16	.2330	+22.30
DoG-HardNet	.4063	-12.96	.4685	-11.38	.4579	-11.03	.4259	-8.31
L2Net	.4529	+1.13	.3972	-20.09	.4456	-8.77	.4005	-8.61
Key.Net-HardNet	.2994	-24.97	.3798	-19.18	.3733	-17.59		
Geodesc	.3752	-10.32	.4390	-8.28	.4323	-9.04	.3983	-7.93
ContextDesc	.3450	-19.44	.4143	-14.69	.3952	-15.23	.3903	-11.15
SOSNet	.3911	-14.88	.4589	-12.30	.4559	-11.93	.4126	-11.28
LogPolarDesc	.3774	-16.04	.4385	-13.68	.4334	-13.34	.4032	-12.76
SuperPoint (2k)	.1898	-19.55	.2375	-11.02	.2256	-13.90	.2957	-0.08
LF-Net (2k)	.1734	-10.85	.2197	-2.51	.2091	-3.40	.2929	-2.5
D2-Net (SS)	.1058	-26.10	.1410	-13.96	.1262	-19.10	.1991	-3.18
D2-Net (MS)	.0855	-49.41	.1102	-39.99	.1007	-41.80	.1673	-21.93

Table 3. **Outlier pre-filtering with CNe – Test set.** We report mAP at 10° with CNe, on stereo and multi-view, and its increase in performance w.r.t. Table 2 – positive Δ meaning CNe helps. When using CNe, we disable the ratio test.

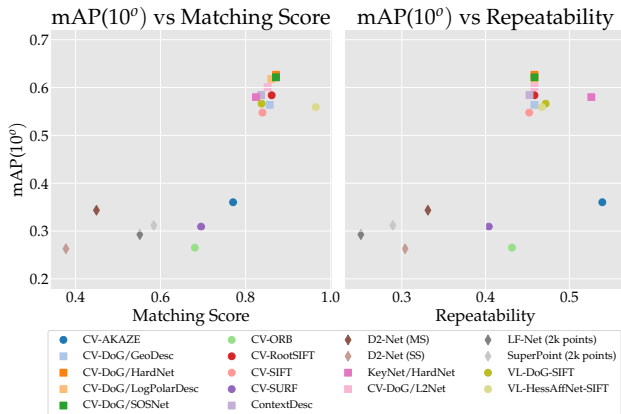


Figure 11. **Downstream vs. traditional metrics.** We cross-reference stereo mAP at 10° with repeatability and matching score, with a 3-pixel threshold, computed as outlined in Section 4.

ducing similar inlier ratios to the ratio test – 43-75% with the ratio test, and 38-73% with CNe, which suggests that CNe preserves more *true* inliers than the ratio test. This margin is more pronounced on the multi-view task – in fact, nearly all classical methods benefit from it, up to 30% relative. However, it is damaging with most learned descriptors, even those operating on DoG keypoints. We hypothesize this might be because the models performed better on the ‘classical’ keypoints it was trained with – [85] reports that re-training them for a specific feature helps.

On the effect of local feature orientation. In contrast with classical methods, which estimate the orientation of each keypoint, modern, end-to-end pipelines [31, 33, 71] often skip this step, assuming that the images are roughly aligned (upright), with the descriptor shouldering the increased invariance requirements. As our images meet this condition, we experiment with setting the orientation of keypoints to a fixed value (0). We list the results in Table 4. This allows us

	CV-SIFT		HardNet		LogpolarDesc		SOSNet	
	NI	mAP(10)	NI	mAP(10)	NI	mAP(10)	NI	mAP(10)
Standard	222.7	.4608	342.2	.5286	366.0	.5080	319.8	.5233
Upright	177.2	.4569	363.9	.5354	381.1	.5166	339.1	.5332
Δ (%)	-20.43	-0.85	+6.34	+1.29	+4.13	+1.69	+6.04	+1.89
Upright++	275.3	.4823	409.3	.5436	430.2	.5250	379.5	.5396
Δ (%)	+18.90	+4.67	+19.61	+2.84	+17.54	+3.35	+18.67	+3.11

Table 4. **Upright features.** We report (NI) the number of inliers and mAP at 10° for stereo, with DEGENSAC. As DoG may return multiple orientations for the same point [48] (about 15%), we report: **(top)** with orientation estimation; **(middle)** setting the orientation to zero while removing duplicates; and **(bottom)** adding new points until hitting the 8000-feature budget.

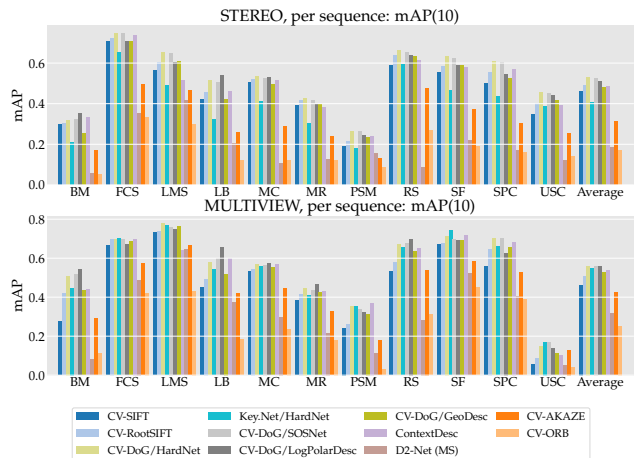


Figure 12. **Breakdown by scene.** Results vary drastically between scenes. Please refer to the appendix for a legend.

to remove keypoints with duplicate orientations, effectively increasing our feature budget and improving performance across the board – albeit by a small margin.

Pose mAP vs. traditional metrics. Fig. 11 shows how repeatability and matching score correlate with mAP. While the matching score results seem sensible, repeatability is harder to interpret (as explained in Section 4, our implementation differs from the standard). ContextDesc performs well despite poor repeatability, and AKAZE obtains the best repeatability but performs poorly in terms of mAP and matching score, which indicates the descriptor may hurt its performance. We compute these metrics at a 3-pixel threshold, and provide more granular results in the appendix.

Breakdown by scene. Results may vary drastically from scene to scene, as show in Fig. 12. A given method may also perform better on some than others – for instance, D2-Net nears the state of the art on ‘Lincoln Memorial Statue’, but is 5x times worse on ‘British Museum’. AKAZE and ORB show similar behaviour. We believe this can provide valuable insights on limitations and failure cases.

7. Conclusions

We introduce a comprehensive benchmark for local features and robust estimation algorithms. The modular structure of its pipeline allows to easily integrate, configure, and combine methods and heuristics. We demonstrate this by evaluating dozens of popular algorithms, from seminal works to the cutting edge of machine learning research, and show that classical solutions may still outperform the perceived state of the art with proper settings.

The experiments carried out through the benchmark and reported in this paper have already revealed unexpected, non-intuitive properties of various components of the SfM pipeline, which will benefit SfM development, *e.g.*, the need to tune RANSAC to the particular feature detector and descriptor and to select specific settings for a particular RANSAC variant. Other surprising facts have been uncovered by our tests, such as that the optimal set-ups across different tasks (stereo and multiview) may differ, or that end-to-end methods are very sensitive to the scene.

Our work is open-sourced and makes the basis of an open challenge for image matching with sparse methods.

Acknowledgements

This work was partially supported by the Natural Sciences and Engineering Research Council of Canada (NSERC) Discovery Grant “Deep Visual Geometry Machines” (RGPIN-2018-03788), by systems supplied by Compute Canada, and by Google’s Visual Positioning Service. DM and JM were supported by OP VVV funded project CZ.02.1.01/0.0/0.0/16 019/0000765 “Research Center for Informatics”. DM was also supported by CTU student grant SGS17/185/OHK3/3T/13 and by the Austrian Ministry for Transport, Innovation and Technology, the Federal Ministry for Digital and Economic Affairs, and the Province of Upper Austria in the frame of the COMET center SCCH. AM was supported by Swiss National Science Foundation.

References

- [1] H. Aanaes, A. L. Dahl, and K. Steenstrup Pedersen. Interesting Interest Points. *IJCV*, 97:18–35, 2012. 2
- [2] H. Aanaes and F. Kahl. Estimation of Deformable Structure and Motion. In *Vision and Modelling of Dynamic Scenes Workshop*, 2002. 6
- [3] S. Agarwal, N. Snavely, I. Simon, S.M. Seitz, and R. Szeliski. Building Rome in One Day. In *ICCV*, 2009. 1, 2
- [4] P. F. Alcantarilla, J. Nuevo, and A. Bartoli. Fast Explicit Diffusion for Accelerated Features in Nonlinear Scale Spaces. In *BMVC*, 2013. 2, 3
- [5] Anonymous. DeepSfM: Structure From Motion Via Deep Bundle Adjustment. In *Submission to ICLR*, 2020. 2
- [6] Relja Arandjelovic. Three things everyone should know to improve object retrieval. In *CVPR*, 2012. 3
- [7] Relja Arandjelovic, Petr Gronat, Akihiko Torii, Tomas Padlla, and Josef Sivic. NetVLAD: CNN Architecture for Weakly Supervised Place Recognition. In *CVPR*, 2016. 1
- [8] Hernan Badino, Daniel Huber, and Takeo Kanade. The CMU Visual Localization Data Set. <http://3dvis.ri.cmu.edu/data-sets/localization>, 2011. 2
- [9] V. Balntas, K. Lenc, A. Vedaldi, and K. Mikolajczyk. HPatches: A Benchmark and Evaluation of Handcrafted and Learned Local Descriptors. In *CVPR*, 2017. 2, 7
- [10] Vassileios Balntas, Shuda Li, and Victor Prisacariu. ReLocNet: Continuous Metric Learning Relocalisation using Neural Nets. In *The European Conference on Computer Vision (ECCV)*, September 2018. 1
- [11] V. Balntas, E. Riba, D. Ponsa, and K. Mikolajczyk. Learning Local Feature Descriptors with Triplets and Shallow Convolutional Neural Networks. In *BMVC*, 2016. 2
- [12] Daniel Barath and Ji Matas. Graph-cut ransac. In *The IEEE Conference on Computer Vision and Pattern Recognition (CVPR)*, June 2018. 2, 4
- [13] Axel Barroso-Laguna, Edgar Riba, Daniel Ponsa, and Krystian Mikolajczyk. Key.Net: Keypoint Detection by Handcrafted and Learned CNN Filters. In *Proceedings of the 2019 IEEE/CVF International Conference on Computer Vision*, 2019. 2, 3
- [14] A. Baumberg. Reliable Feature Matching Across Widely Separated Views. In *CVPR*, pages 774–781, 2000. 3, 6
- [15] H. Bay, T. Tuytelaars, and L. Van Gool. SURF: Speeded Up Robust Features. In *ECCV*, 2006. 2, 3
- [16] P. R. Beaudet. Rotationally invariant image operators. In *Proceedings of the 4th International Joint Conference on Pattern Recognition*, pages 579–583, Kyoto, Japan, Nov. 1978. 3, 6
- [17] Jia-Wang Bian, Yu-Huan Wu, Ji Zhao, Yun Liu, Le Zhang, Ming-Ming Cheng, and Ian Reid. An Evaluation of Feature Matchers for Fundamental Matrix Estimation. In *BMVC*, 2019. 2
- [18] Eric Brachmann and Carsten Rother. Neural-Guided RANSAC: Learning Where to Sample Model Hypotheses. In *ICCV*, 2019. 2
- [19] G. Bradski. The OpenCV Library. *Dr. Dobb’s Journal of Software Tools*, 2000. 4
- [20] M. Brown, G. Hua, and S. Winder. Discriminative Learning of Local Image Descriptors. *PAMI*, 2011. 1, 2, 7
- [21] M. Brown and D. Lowe. Automatic Panoramic Image Stitching Using Invariant Features. *IJCV*, 74:59–73, 2007. 2
- [22] Mai Bui, Christoph Baur, Nassir Navab, Slobodan Ilic, and Shadi Albarqouni. Adversarial Networks for Camera Pose Regression and Refinement. In *The IEEE International Conference on Computer Vision (ICCV) Workshops*, Oct 2019. 1
- [23] Ondřej Chum and Jiří Matas. Matching with PROSAC - Progressive Sample Consensus. In *CVPR*, pages 220–226, June 2005. 2
- [24] Ondřej Chum, Jiří Matas, and Josef Kittler. Locally Optimized RANSAC. In *PR*, 2003. 2
- [25] Ondřej Chum, Jiří Matas, and Josef Kittler. Locally optimized ransac. In *Pattern Recognition*, 2003. 4

- [26] Ondrej Chum, Tomas Werner, and Jiri Matas. Two-View Geometry Estimation Unaffected by a Dominant Plane. In *CVPR*, 2005. 2, 4
- [27] Hainan Cui, Xiang Gao, Shuhan Shen, and Zhanyi Hu. Hsfm: Hybrid structure-from-motion. In *CVPR*, July 2017. 2
- [28] Zheng Dang, Kwang Moo Yi, Yinlin Hu, Fei Wang, Pascal Fua, and Mathieu Salzmann. Eigendecomposition-Free Training of Deep Networks with Zero Eigenvalue-Based Losses. In *ECCV*, 2018. 4
- [29] Jana Noskova Daniel Barath, Jiri Matas. MAGSAC: marginalizing sample consensus. In *CVPR*, 2019. 1, 2, 4
- [30] D. Detone, T. Malisiewicz, and A. Rabinovich. Toward Geometric Deep SLAM. *arXiv preprint arXiv:1707.07410*, 2017. 1
- [31] D. Detone, T. Malisiewicz, and A. Rabinovich. Superpoint: Self-Supervised Interest Point Detection and Description. *CVPR Workshop on Deep Learning for Visual SLAM*, 2018. 1, 2, 3, 8
- [32] J. Dong and S. Soatto. Domain-Size Pooling in Local Descriptors: DSP-SIFT. In *CVPR*, 2015. 6
- [33] M. Dusmanu, I. Rocco, T. Pajdla, M. Pollefeys, J. Sivic, A. Torii, and T. Sattler. D2-Net: A Trainable CNN for Joint Detection and Description of Local Features. In *CVPR*, 2019. 1, 2, 3, 8
- [34] Patrick Ebel, Anastasiia Mishchuk, Kwang Moo Yi, Pascal Fua, and Eduard Trulls. Beyond Cartesian Representations for Local Descriptors. In *ICCV*, 2019. 2, 3, 6
- [35] Vassileios Balntas et al. SILDA: A Multi-Task Dataset for Evaluating Visual Localization. <https://github.com/scape-research/silda>, 2018. 2
- [36] M.A Fischler and R.C. Bolles. Random Sample Consensus: A Paradigm for Model Fitting with Applications to Image Analysis and Automated Cartography. *Communications ACM*, 24(6):381–395, 1981. 1, 2, 4
- [37] P. Gay, V. Bansal, C. Rubino, and A. D. Bue. Probabilistic Structure from Motion with Objects (PSfMO). In *ICCV*, 2017. 2
- [38] Andreas Geiger, Philip Lenz, and Raquel Urtasun. Are we ready for Autonomous Driving? The KITTI Vision Benchmark Suite. In *CVPR*, 2012. 2
- [39] R.I. Hartley. In Defense of the Eight-Point Algorithm. *PAMI*, 19(6):580–593, June 1997. 2
- [40] R. Hartley and A. Zisserman. *Multiple View Geometry in Computer Vision*. Cambridge University Press, 2000. 1
- [41] R. I. Hartley. Projective reconstruction and invariants from multiple images. *IEEE Transactions on Pattern Analysis and Machine Intelligence*, 16(10):1036–1041, Oct 1994. 1, 2
- [42] K. He, Y. Lu, and S. Sclaroff. Local Descriptors Optimized for Average Precision. In *CVPR*, 2018. 1
- [43] J. Heinly, J.L. Schoenberger, E. Dunn, and J-M. Frahm. Reconstructing the World in Six Days. In *CVPR*, 2015. 1, 2, 3
- [44] Karel Lenc and Varun Gulshan and Andrea Vedaldi. VLBenckmarks. <http://www.vlfeat.org/benckmarks/>, 2011. 2
- [45] A. Kendall, M. Grimes, and R. Cipolla. PoseNet: A Convolutional Network for Real-Time 6-DOF Camera Relocalization. In *ICCV*, pages 2938–2946, 2015. 1
- [46] J. Krishna Murthy, Ganesh Iyer, and Liam Paull. grad-SLAM: Dense SLAM meets Automatic Differentiation. *arXiv*, 2019. 2
- [47] Zhengqi Li and Noah Snavely. MegaDepth: Learning Single-View Depth Prediction from Internet Photos. In *CVPR*, 2018. 2
- [48] David G. Lowe. Distinctive Image Features from Scale-Invariant Keypoints. *IJCV*, 20(2):91–110, November 2004. 1, 2, 3, 4, 6, 8, 15
- [49] Zixin Luo, Tianwei Shen, Lei Zhou, Jiahui Zhang, Yao Yao, Shiwei Li, Tian Fang, and Long Quan. ContextDesc: Local Descriptor Augmentation with Cross-Modality Context. In *CVPR*, 2019. 2, 3
- [50] Z. Luo, T. Shen, L. Zhou, S. Zhu, R. Zhang, Y. Yao, T. Fang, and L. Quan. Geodesc: Learning Local Descriptors by Integrating Geometry Constraints. In *ECCV*, 2018. 2, 3
- [51] Simon Lynen, Bernhard Zeisl, Dror Aiger, Michael Bosse, Joel Hesch, Marc Pollefeys, Roland Siegwart, and Torsten Sattler. Large-scale, real-time visual-inertial localization revisited. *arXiv Preprint*, 2019. 1
- [52] Will Maddern, Geoffrey Pascoe, Chris Linegar, and Paul Newman. 1 year, 1000 km: The Oxford RobotCar dataset. *IJRR*, 36(1):3–15, 2017. 2
- [53] J. Matas, O. Chum, M. Urban, and T. Pajdla. Robust Wide-Baseline Stereo from Maximally Stable Extremal Regions. *IVC*, 22(10):761–767, 2004. 3, 6
- [54] K. Mikolajczyk and C. Schmid. A Performance Evaluation of Local Descriptors. *PAMI*, 27(10):1615–1630, 2004. 2
- [55] K. Mikolajczyk, C. Schmid, and A. Zisserman. Human Detection Based on a Probabilistic Assembly of Robust Part Detectors. In *ECCV*, pages 69–82, 2004. 3, 6
- [56] Jiri Matas Milan Pultar, Dmytro Mishkin. Leveraging Outdoor Webcams for Local Descriptor Learning. In *Proceedings of CVWW 2019*, 2019. 7
- [57] A. Mishchuk, D. Mishkin, F. Radenovic, and J. Matas. Working Hard to Know Your Neighbor’s Margins: Local Descriptor Learning Loss. In *NeurIPS*, 2017. 2, 3, 6
- [58] Dmytro Mishkin, Jiri Matas, and Michal Perdoch. MODS: Fast and robust method for two-view matching. *CVIU*, 2015. 6, 15
- [59] D. Mishkin, F. Radenovic, and J. Matas. Repeatability is Not Enough: Learning Affine Regions via Discriminability. In *ECCV*, 2018. 3, 6
- [60] Arun Mukundan, Giorgos Toliás, and Ondrej Chum. Explicit Spatial Encoding for Deep Local Descriptors. In *CVPR*, 2019. 1
- [61] R. Mur-Artal, J. Montiel, and J. Tardós. Orb-Slam: A Versatile and Accurate Monocular Slam System. *IEEE Transactions on Robotics*, 31(5):1147–1163, 2015. 1
- [62] D. Nister. An Efficient Solution to the Five-Point Relative Pose Problem. In *CVPR*, June 2003. 2

- [63] Hyeonwoo Noh, Andre Araujo, Jack Sim, and Tobias Weyand and Bohyung Han. Large-Scale Image Retrieval with Attentive Deep Local Features. In *ICCV*, 2017. 1, 2
- [64] Yuki Ono, Eduard Trulls, Pascal Fua, and Kwang Moo Yi. LF-Net: Learning Local Features from Images. In *NeurIPS*, 2018. 2, 3
- [65] F. Pedregosa, G. Varoquaux, A. Gramfort, V. Michel, B. Thirion, O. Grisel, M. Blondel, P. Prettenhofer, R. Weiss, V. Dubourg, J. Vanderplas, A. Passos, D. Cournapeau, M. Brucher, M. Perrot, and E. Duchesnay. Scikit-learn: Machine learning in Python. *Journal of Machine Learning Research*, 12:2825–2830, 2011. 4
- [66] Stephen M. Pizer, E. Philip Amburn, John D. Austin, Robert Cromartie, Ari Geselowitz, Trey Greer, Bart ter Haar Romeny, John B. Zimmerman, and Karel Zuiderveld. Adaptive histogram equalization and its variations. *Computer vision, graphics, and image processing*, 1987. 15
- [67] M. Pultar, D. Mishkin, and J. Matas. Leveraging Outdoor Webcams for Local Descriptor Learning. In *Computer Vision Winter Workshop*, 2019. 2, 7
- [68] C.R. Qi, H. Su, K. Mo, and L.J. Guibas. Pointnet: Deep Learning on Point Sets for 3D Classification and Segmentation. In *CVPR*, 2017. 4
- [69] Filip Radenovic, Georgios Toliás, and Ondra Chum. CNN image retrieval learns from BoW: Unsupervised fine-tuning with hard examples. In *ECCV*, 2016. 1
- [70] R. Ranftl and V. Koltun. Deep Fundamental Matrix Estimation. In *ECCV*, 2018. 2, 4
- [71] J. Revaud, P. Weinzaepfel, C. De Souza, N. Pion, G. Csurka, Y. Cabon, and M. Humenberger. R2D2: Repeatable and Reliable Detector and Descriptor. In *arXiv Preprint*, 2019. 8
- [72] Jérôme Revaud, Philippe Weinzaepfel, César Roberto de Souza, Noe Pion, Gabriela Csurka, Yohann Cabon, and Martin Humenberger. R2D2: Repeatable and Reliable Detector and Descriptor. In *NeurIPS*, 2019. 2
- [73] E. Rublee, V. Rabaud, K. Konolidge, and G. Bradski. ORB: An Efficient Alternative to SIFT or SURF. In *ICCV*, 2011. 2, 3, 6
- [74] Torsten Sattler, Bastian Leibe, and Leif Kobbelt. Improving Image-Based Localization by Active Correspondence Search. In *ECCV*, 2012. 1
- [75] T. Sattler, W. Maddern, C. Toft, A. Torii, L. Hammarstrand, E. Stenborg, D. Safari, M. Okutomi, M. Pollefeys, J. Sivic, F. Kahl, and T. Pajdla. Benchmarking 6DOF Outdoor Visual Localization in Changing Conditions. In *CVPR*, 2018. 1, 2
- [76] Torsten Sattler, Tobias Weyand, Bastian Leibe, and Leif Kobbelt. Image Retrieval for Image-Based Localization Revisited. In *BMVC*, 2012. 2
- [77] Torsten Sattler, Qunjie Zhou, Marc Pollefeys, and Laura Leal-Taixe. Understanding the Limitations of CNN-based Absolute Camera Pose Regression. In *CVPR*, 2019. 1
- [78] N. Savinov, A. Seki, L. Ladicky, T. Sattler, and M. Pollefeys. Quad-Networks: Unsupervised Learning to Rank for Interest Point Detection. *CVPR*, 2017. 2
- [79] J.L. Schönberger and J.M. Frahm. Structure-From-Motion Revisited. In *CVPR*, 2016. 1, 2, 3, 4, 6
- [80] J.L. Schönberger, H. Hardmeier, T. Sattler, and M. Pollefeys. Comparative Evaluation of Hand-Crafted and Learned Local Features. In *CVPR*, 2017. 2
- [81] Yunxiao Shi, Jing Zhu, Yi Fang, Kuochin Lien, and Junli Gu. Self-Supervised Learning of Depth and Ego-motion with Differentiable Bundle Adjustment. *arXiv Preprint*, 2019. 2
- [82] E. Simo-serra, E. Trulls, L. Ferraz, I. Kokkinos, P. Fua, and F. Moreno-Noguer. Discriminative Learning of Deep Convolutional Feature Point Descriptors. In *ICCV*, 2015. 2
- [83] C. Strecha, W.V. Hansen, L. Van Gool, P. Fua, and U. Thoennessen. On Benchmarking Camera Calibration and Multi-View Stereo for High Resolution Imagery. In *CVPR*, 2008. 2
- [84] J. Sturm, N. Engelhard, F. Endres, W. Burgard, and D. Cremers. A Benchmark for the Evaluation of RGB-D SLAM Systems. In *IROS*, 2012. 4
- [85] Weiwei Sun, Wei Jiang, Eduard Trulls, Andrea Tagliasacchi, and Kwang Moo Yi. Attentive Context Normalization for Robust Permutation-Equivariant Learning. In *arXiv Preprint*, 2019. 2, 4, 8
- [86] Chengzhou Tang and Ping Tan. Ba-Net: Dense Bundle Adjustment Network. In *ICLR*, 2019. 2
- [87] Keisuke Tateno, Federico Tombari, Iro Laina, and Nassir Navab. Cnn-slam: Real-time dense monocular slam with learned depth prediction. In *CVPR*, July 2017. 2
- [88] B. Thomee, D.A. Shamma, G. Friedland, B. Elizalde, K. Ni, D. Poland, D. Borth, and L. Li. YFCC100M: the New Data in Multimedia Research. In *CACM*, 2016. 3
- [89] Y. Tian, B. Fan, and F. Wu. L2-Net: Deep Learning of Discriminative Patch Descriptor in Euclidean Space. In *CVPR*, 2017. 2, 3
- [90] Yurun Tian, Xin Yu, Bin Fan, Fuchao Wu, Huub Heijnen, and Vassileios Balntas. SOSNet: Second Order Similarity Regularization for Local Descriptor Learning. In *CVPR*, 2019. 1, 2, 3
- [91] Giorgos Toliás, Yannis Avrithis, and Hervé Jégou. Image Search with Selective Match Kernels: Aggregation Across Single and Multiple Images. *IJCV*, 116(3):247–261, Feb 2016. 1
- [92] P.H.S. Torr and A. Zisserman. MLESAC: A New Robust Estimator with Application to Estimating Image Geometry. *CVIU*, 78:138–156, 2000. 2
- [93] B. Triggs, P. Mclauchlan, R. Hartley, and A. Fitzgibbon. Bundle Adjustment – A Modern Synthesis. In *Vision Algorithms: Theory and Practice*, pages 298–372, 2000. 1
- [94] Andrea Vedaldi and Brian Fulkerson. Vlfeat: An open and portable library of computer vision algorithms. In *Proceedings of the 18th ACM International Conference on Multimedia*, MM '10, pages 1469–1472, 2010. 3
- [95] Y. Verdie, K. M. Yi, P. Fua, and V. Lepetit. TILDE: A Temporally Invariant Learned DETector. In *CVPR*, 2015. 2
- [96] S. Vijayanarasimhan, S. Ricco, C. Schmid, R. Sukthankar, and K. Fragkiadaki. Sfm-Net: Learning of Structure and Motion from Video. *arXiv Preprint*, 2017. 2

- [97] X. Wei, Y. Zhang, Y. Gong, and N. Zheng. Kernelized Subspace Pooling for Deep Local Descriptors. In *CVPR*, 2018. [1](#)
- [98] Changchang Wu. Towards Linear-Time Incremental Structure from Motion. In *3DV*, 2013. [2](#), [6](#)
- [99] Kwang Moo Yi, Eduard Trulls, Vincent Lepetit, and Pascal Fua. LIFT: Learned Invariant Feature Transform. In *ECCV*, 2016. [2](#)
- [100] K. M. Yi, E. Trulls, Y. Ono, V. Lepetit, M. Salzmann, and P. Fua. Learning to Find Good Correspondences. In *CVPR*, 2018. [2](#), [3](#), [4](#), [7](#), [13](#), [17](#)
- [101] S. Zagoruyko and N. Komodakis. Learning to Compare Image Patches via Convolutional Neural Networks. In *CVPR*, 2015. [6](#)
- [102] Jiahui Zhang, Dawei Sun, Zixin Luo, Anbang Yao, Lei Zhou, Tianwei Shen, Yurong Chen, Long Quan, and Hongen Liao. Learning Two-View Correspondences and Geometry Using Order-Aware Network. *ICCV*, 2019. [2](#), [3](#), [4](#)
- [103] Xu Zhang, Felix X. Yu, Svebor Karaman, and Shih-Fu Chang. Learning Discriminative and Transformation Covariant Local Feature Detectors. In *The IEEE Conference on Computer Vision and Pattern Recognition (CVPR)*, July 2017. [2](#)
- [104] Chen Zhao, Zhiguo Cao, Chi Li, Xin Li, and Jiaqi Yang. NM-Net: Mining Reliable Neighbors for Robust Feature Correspondences. In *CVPR*, 2019. [2](#), [4](#)
- [105] Qunjie Zhou, Torsten Sattler, Marc Pollefeys, and Laura Leal-Taixe. To learn or not to learn: Visual localization from essential matrices. *arXiv Preprint*, 2019. [1](#)
- [106] Siyu Zhu, Runze Zhang, Lei Zhou, Tianwei Shen, Tian Fang, Ping Tan, and Long Quan. Very Large-Scale Global SfM by Distributed Motion Averaging. In *CVPR*, June 2018. [1](#), [2](#)
- [107] C.L. Zitnick and K. Ramnath. Edge Foci Interest Points. In *ICCV*, 2011. [2](#)

8. Appendix

In this section we provide details about our data, experiments, and qualitative results that were omitted from the main paper due to space constraints. All results are on the validation set, unless stated otherwise.

8.1. Dataset details

We provide over 25k images for training, including 2D/3D points, camera poses, and dense depth estimates. We use ‘sacre_coeur’ and ‘st_peters_square’ for the validation and ablation test experiments of Section 5. We generate the validation data following the same procedure we used for the test data, outlined in Section 3. These two subsets will also be released, so that the validation results are reproducible and comparable. Additionally, We use ‘Notre Dame Front Facade’ and ‘Buckingham Palace’ to retrain CNe [100], which was originally trained on one of our validation sequences, as outlined in Section 4. The rest of the ‘training’ sequences are not used in this paper. We test the new models on the test set and observe that performance improves.

The test scenes as listed in Table 5, along with the acronym used in Fig. 12. Note that we only release 100 images for each, to keep the load manageable, as every possible combination of two images needs to be considered – the ground truth, which will remain behind a public evaluation server, is computed with the full image set. Links for both will be provided after the review phase.

8.2. Co-visibility metric example

In Section 3 we introduce how we compute a simple co-visibility measure to determine how much content is shared between two images, by extracting the 3D keypoints in common across both images, projecting them into the camera plane, and computing their bounding box – Fig. 13 shows an example. We also plot the co-visibility histograms for every scene in Fig. 14. This value gives an indication of how ‘hard’ each scene is, accounting by changes in scale, but not necessarily large-scale occlusions – notice, for instance, how USC (‘United States Capitol’) is one of the hardest scenes in the breakdown in Fig. 12. For stereo, we set the minimum co-visibility threshold to 0.1.

8.3. Breakdown by co-visibility threshold

Here we show results for stereo at different co-visibility thresholds, for different features in Fig. 15, and for different RANSAC methods in Fig. 16. Performance for all local feature and RANSAC variants increases about 20% (absolute) as the co-visibility threshold increases from 0.1 to 0.6, where SuperPoint benefits the most (a 60% relative performance boost). By contrast, we do not observe significant variations across different RANSAC methods,

Name	Images	3D points
brandenburg_gate	1363	100040
buckingham_palace	1676	234052
colosseum_exterior	2063	259807
grand_place_brussels	1083	229788
hagia_sophia_interior	888	235541
notre_dame_front_facade	3765	488895
palace_of_westminster	983	115868
pantheon_exterior	1401	166923
prague_old_town_square	2316	558600
sacre_coeur (SC)	1179	140659
st_peters_square (SPS)	2504	232329
taj_mahal	1312	94121
temple_nara_japan	904	92131
trevi_fountain	3191	580673
westminster_abbey	1061	198222
Total	25.6k	3.7M

Table 5. Dataset – Training and validation.

Name	Images	3D points
british_museum (BM)	660	73569
florence_cathedral_side (FCS)	108	44143
lincoln_memorial_statue (LMS)	850	58661
london_bridge (LB)	629	72235
milan_cathedral (MC)	124	33905
mount_rushmore (MR)	138	45350
piazza_san_marco (PSM)	249	95895
reichstag (RS)	75	17823
sagrada_familia (SF)	401	120723
st_pauls_cathedral (SPC)	615	98872
united_states_capitol (USC)	258	35095
Total	4107	696k

Table 6. Dataset – Test.

with DEGENSAC and MAGSAC showing very similar performance. Note that at co-visibility 0 some image pairs may not be matchable, and that results at high co-visibility thresholds are noisy as we have few samples for them – we

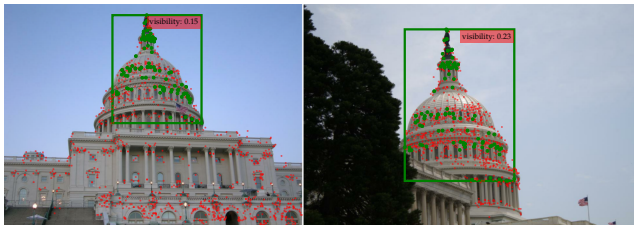


Figure 13. Co-visibility computation example. We project the 3D points obtained with COLMAP into two images, and color them green if they are seen from both views, and red otherwise. The ‘visibility’ value is the ratio between the area of the bounding box of the shared points, and that of the image. The ‘co-visibility’ value for these two images is the smallest of the two.

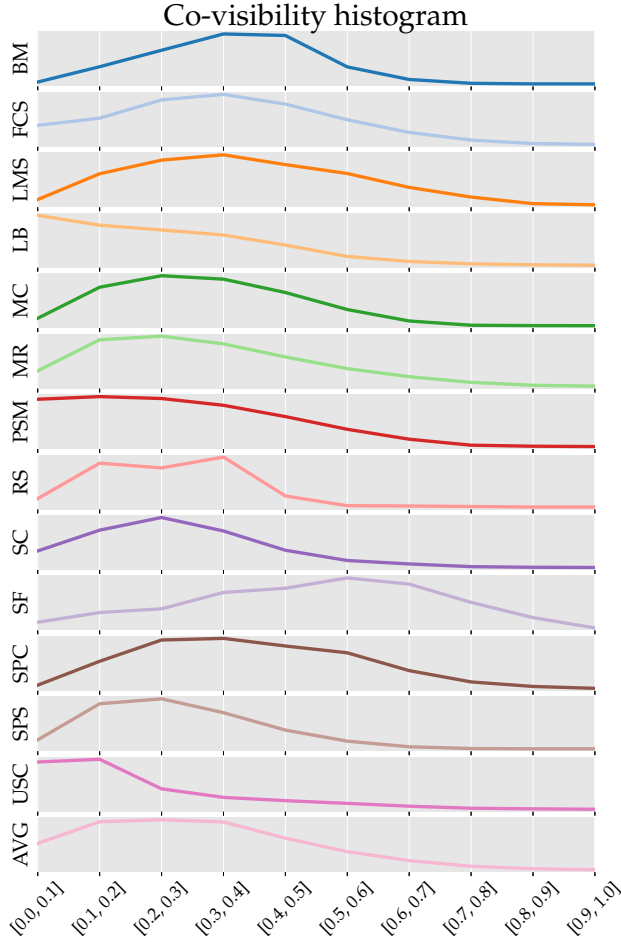


Figure 14. **Co-visibility histogram** – Breakdown for each scene in the validation and test sets. Notice how the statistics may significantly change from scene to scene.

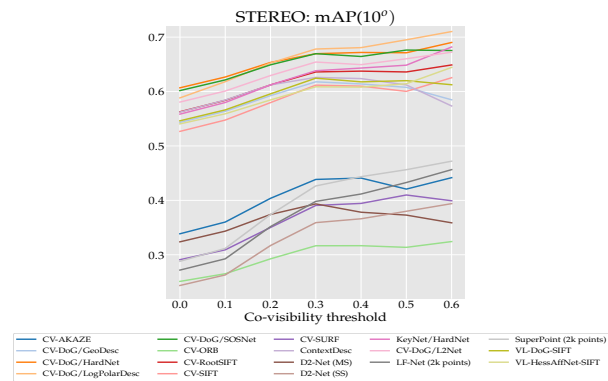


Figure 15. **Local feature performance by co-visibility** – We show mAP at 10° on the stereo task at different co-visibility thresholds for different local feature types, on the validation set.

do not plot co-visibility values above 0.6 as these bins are very sparsely populated.

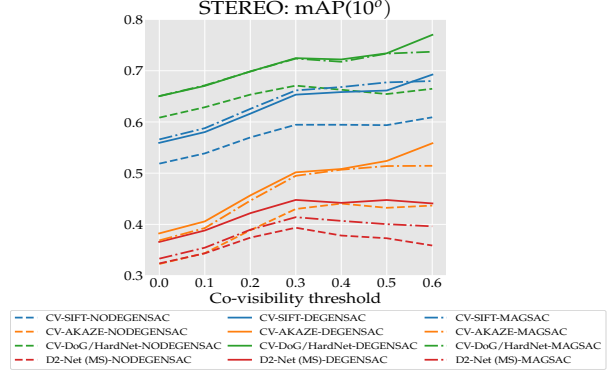


Figure 16. **RANSAC performance by co-visibility** – We show mAP at 10° on the stereo task at different co-visibility thresholds for different RANSAC methods, on the validation set.

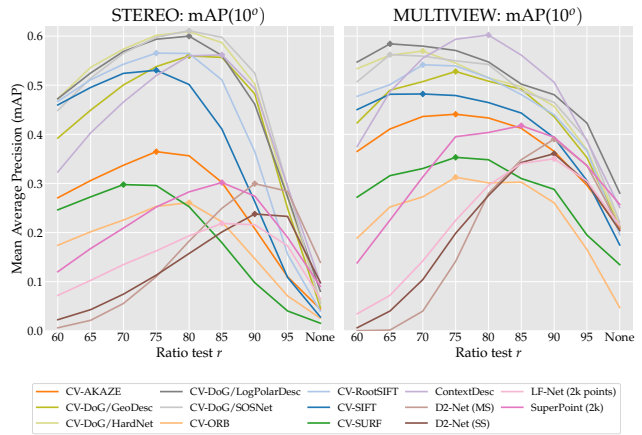


Figure 17. **Optimal ratio test for matching with ‘either’** – Equivalent to Fig. 6 in the paper, but for the ‘either’ matching strategy.

8.4. Alternative matching strategies

As discussed in the main paper, the best matching strategy is bidirectional matching with ‘both’, and the only one we consider for the vast majority of the experiments. Fig. 7 (in the main paper) shows that performance is slightly worse with unidirectional matching. In this section we evaluate the ‘either’ strategy as an alternative – results are shown in Fig. 17, which shows that performance is typically worse. It also requires more strict (lower) ratio test thresholds in order to restrict the number of matches, which is noticeably higher, and slows RANSAC down very significantly, even for the same limit of iterations.

8.5. Number of inliers per step

We report the number of input matches and their resulting inliers for the stereo task in Table 7. We list: the number of input matches; the number of inliers produced by each method (they may still contain outliers); their ratio; and the mAP at 10° . We use PyRANSAC with optimal settings for

Method	# matches	# inliers	Ratio (%)	mAP(10°)
CV-SIFT	328.3	113.0	34.4	0.548
CV- $\sqrt{\text{SIFT}}$	331.6	131.4	39.6	0.584
SURF	221.5	77.4	35.0	0.309
AKAZE	369.1	143.5	38.9	0.360
ORB	193.4	74.7	38.6	0.265
DoG-HardNet	433.1	173.1	40.0	0.627
L2Net	368.0	144.0	39.1	0.601
GeoDesc	322.6	133.4	41.3	0.564
ContextDesc	560.8	240.1	42.8	0.584
SOSNet	391.7	161.8	41.3	0.621
LogPolarDesc	522.8	175.2	33.5	0.618
SuperPoint (2k)	202.0	62.6	31.0	0.312
LF-Net (2k)	165.9	73.2	44.1	0.293
D2-Net (SS)	657.3	148.9	22.7	0.263
D2-Net (MS)	601.7	161.7	26.9	0.343

Table 7. **Number of inliers with optimal settings** – With 8000 features and optimal ratio test and PyRANSAC settings, on the validation set.

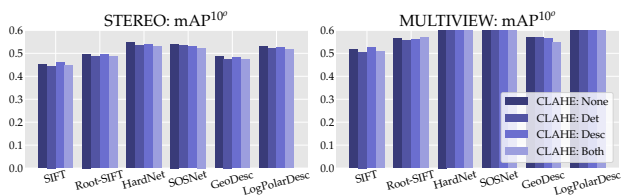


Figure 18. **Image pre-processing with CLAHE.**

each method, including the ratio test, using bidirectional matching with the ‘both’ strategy. We see that inlier-to-outlier ratios hover around 40% for all feature types except D2-Net, which seems adequate for RANSAC, and might explain why D2-Net, which is not amenable to the ratio test, performs poorly on our benchmark.

8.6. Image pre-processing

Contrast normalization is key to invariance against illumination changes – local feature methods typically apply some normalization strategy over small patches. Therefore, we experiment with contrast-limited adaptive histogram equalization (CLAHE) [66], as implemented in OpenCV. We apply it to SIFT and to several learned descriptors, and display the results in Fig. 18. Performance decreases for all learned methods, presumably because they are not trained for it. Contrary to our initial expectations, SIFT does not benefit much from it: the only significant increase in performance comes from applying it for descriptor extraction, at 2.4% relative for stereo and 1.9% relative for multi-view. This might be due to the small number of night-time images in our data. It also falls in line with the observations of J. Dong *et al.* in ‘Multi-View Feature Engineering and

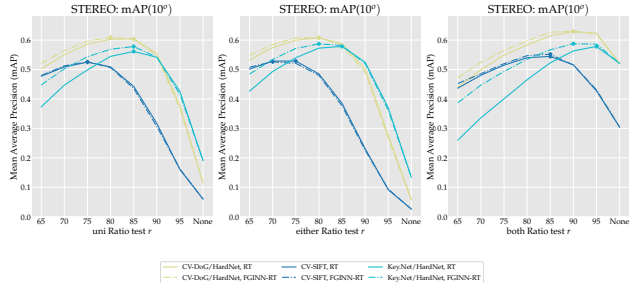


Figure 19. **FGINN vs. standard ratio test** – Ratio test with FGINN is drawn with a dashed line, and the standard ratio test (RT) with a solid line. With FGINN, the valid range for r (the ratio test threshold) is significantly wider, but the best performance with the ‘both’ matching strategy is not significantly better than for the standard ratio test.

Learning’, CVPR 2015, which show that SIFT descriptors are actually optimal under certain assumptions.

8.7. Optimal settings breakdown

We summarize the optimal hyperparameter combinations from Figs. 4, 5 and 6, for clarity, in Table 8. We set the confidence value to $\tau=0.999999$ for all RANSAC variants.

8.8. Feature matching with advanced ratio test

We also compared the benefits of applying first-geometrically-inconsistent-neighbor-ratio (FGINN) [58] to DoG/SIFT, DoG/HardNet and Key.Net/HardNet, against Lowe’s standard ratio test rule [48]. FGINN performs the ratio-test with second-nearest neighbors that are “far enough” from the putative match (10 pixels in [58]). In other words, it loosens the test to allow for nearby-thus-similar points. We test it for 3 matching strategies: unidirectional (‘uni’), ‘both’ and ‘either’. We report the results in Fig. 19. As shown, FGINN provides minor improvements over the standard ratio test in case of unidirectional matching, and not as much when ‘both’ is used. It also behaves differently compared to the standard strategy, in that performance at stricter thresholds degrades less.

8.9. Finding the optimal support region

As outlined in Section 6, we find that the recommended support region used to extract deep descriptors is already optimal, or near so. We plot these results in Fig. 20. Interestingly, SIFT descriptors do benefit from increasing the scaling factor from 12 to 16, but the increase in performance is small. This suggests that deep descriptors such as HardNet might also be able to increase performance slightly training on larger patches.

Method	PyRANSAC		DEGENSAC		GC-RANSAC		MAGSAC		Ratio Test	
	η	mAP(10 $^\circ$)	η	mAP(10 $^\circ$)	η	mAP(10 $^\circ$)	η	mAP(10 $^\circ$)	Stereo	Multiview
CV-AKAZE	0.25	0.3438	0.75	0.4058	0.75	0.3846	1.5	0.3928	0.85	0.90
CV-DoG/GeoDesc	0.2	0.5078	0.5	0.5733	0.75	0.5604	1.5	0.5707	0.90	0.85
CV-DoG/HardNet	0.25	0.6288	0.5	0.6705	0.5	0.6629	1.5	0.6715	0.90	0.80
CV-DoG/LogPolarDesc	0.2	0.5732	0.5	0.6404	0.5	0.6391	1.5	0.6411	0.90	0.80
CV-DoG/SOSNet	0.25	0.5701	0.5	0.6423	0.75	0.6354	1.5	0.6417	0.90	0.85
CV-ORB	0.75	0.2359	1	0.2805	1.25	0.2568	2	0.2652	0.85	0.90
CV-RootSIFT	0.25	0.5638	0.5	0.6164	0.5	0.6086	1.25	0.6188	0.85	0.85
CV-SIFT	0.25	0.5386	0.5	0.5802	0.5	0.5775	1.25	0.5878	0.85	0.80
CV-SURF	0.75	0.3052	0.75	0.3381	0.75	0.3127	2	0.3248	0.85	0.90
ContextDesc	0.5	0.6058	0.5	0.6331	0.5	0.6066	2	0.6201	0.95	0.90
D2-Net (MS)	1	0.3434	2	0.3881	2	0.3599	5	0.3545	N/A	N/A
D2-Net (SS)	1	0.2629	2	0.2854	2	0.2720	7.5	0.2581	N/A	N/A
KeyNet/Hardnet	0.5	0.5801	0.75	0.6313	0.75	0.6268	2	0.6240	0.95	0.85
L2Net	0.2	0.6018	0.5	0.6379	0.5	0.6293	1.5	0.6376	0.90	0.80
LF-Net (2k)	1	0.2925	1	0.3137	1	0.3033	4	0.3063	0.95	0.95
SuperPoint (2k)	0.75	0.3311	1	0.3533	1	0.3247	3	0.3413	0.95	0.90
VL-DoG-SIFT	0.25	0.5577	0.5	0.5987	0.5	0.5853	1.5	0.5995	0.85	0.80
VL-DoGAff-SIFT	0.25	0.5648	0.5	0.6029	0.5	0.5889	1.5	0.6034	0.85	0.80
VL-Hess-SIFT	0.2	0.5719	0.5	0.6044	0.5	0.5990	1.5	0.6087	0.85	0.80
VL-HessAffNet-SIFT	0.25	0.5784	0.5	0.6130	0.5	0.6074	1	0.6165	0.85	0.80

Table 8. **Optimal hyper-parameter combinations** – The number of RANSAC iterations Γ is set to 250k for PyRANSAC, 50k for DEGENSAC, and 10k for both GC-RANSAC and MAGSAC. We use 8000 features (2k for LF-Net and SuperPoint) with bidirectional matching with the ‘both’ strategy.

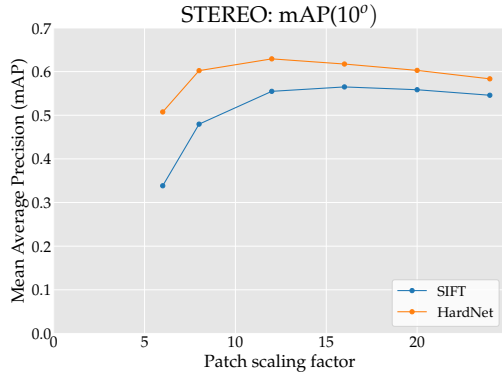


Figure 20. **Scaling the descriptor support region** – Performance with SIFT and HardNet descriptors, applying a scaling factor λ to the keypoint scale (note that OpenCV’s default value is $\lambda=12$).

8.10. Breakdown by (pixel) error threshold

In Fig. 11 in the main paper we plot repeatability and matching score at a fixed error threshold of 3 pixels. In Fig. 21 we show them at different pixel thresholds. Note that repeatability is typically lower than matching score, which might be counter-intuitive as the latter is more strict – we compute repeatability with the raw set of keypoints, whereas the matching score is computed with optimal matching settings (bidirectional matching with the ‘both’ strategy and ratio test), which results in a much smaller pool, from about 8000 keypoints to 150-600 matches (see Table 7). This better isolates the performance of the detector and the descriptor, where it matters.

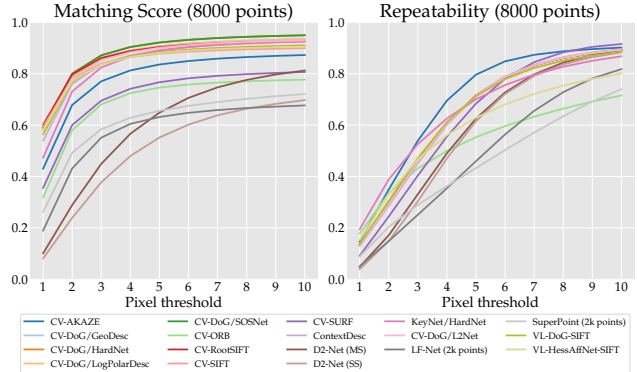


Figure 21. **Classical metrics by threshold** – We show repeatability and matching score computed at different pixel thresholds.

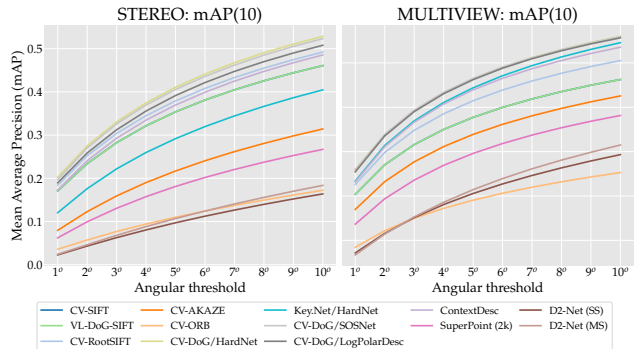


Figure 22. **Breakdown by angular threshold** – We compute mAP with finer granularity. Results are consistent across thresholds.

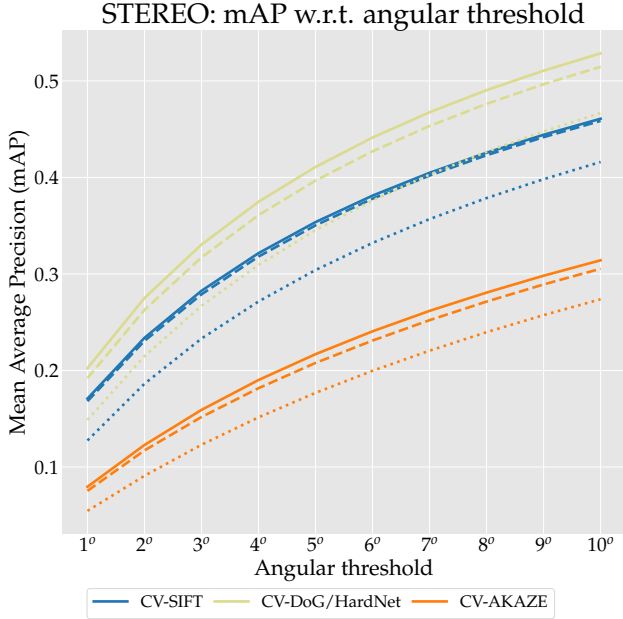


Figure 23. **Breakdown by angular threshold** – We plot RANSAC performance at different angular error thresholds.

	m_{in}	m_{cn}	m_{out}	Stereo mAP(10°)	Multi-view mAP(10°)
RANSAC			110.23	0.5154	
NODEGENSAC			96.99	0.5386	
DEGENSAC	226.15	226.15	139.38	0.5802	0.5132
GC-RANSAC			161.08	0.5775	
MAGSAC			169.30	0.5878	
CNe+RANSAC			165.29	0.5384	
CNe+NODEGENSAC			143.65	0.5685	
CNe+DEGENSAC	1814.13	369.97	213.25	0.6155	0.5860
CNe+GC-RANSAC			253.26	0.5894	
CNe+MAGSAC			272.08	0.5985	

Table 9. **Outlier pre-filtering with CNe** – Results on the validation set, including mAP and the number of matches, from the feature matcher (m_{in}), from outlier pre-filtering with Context Networks (CNe) (m_{cn}), and after stereo (m_{out}). Note that m_{cn} is the input to *both* tasks, and m_{out} is the output of the *stereo* task (see pipeline in Fig. 3).

8.11. Breakdown by (angular) error threshold

We summarize pose accuracy by mAP at 10° (optionally, at 5°), in order to have a single number. In this section we show how performance varies across different error thresholds. Fig. 22 shows how it affects different local feature types, and Fig. 23 shows how it affects different RANSAC variants, with SIFT. Better features perform better at any threshold, at least up to 10° . The same applies to differences between RANSAC methods. Differences between methods are more pronounced for multi-view.

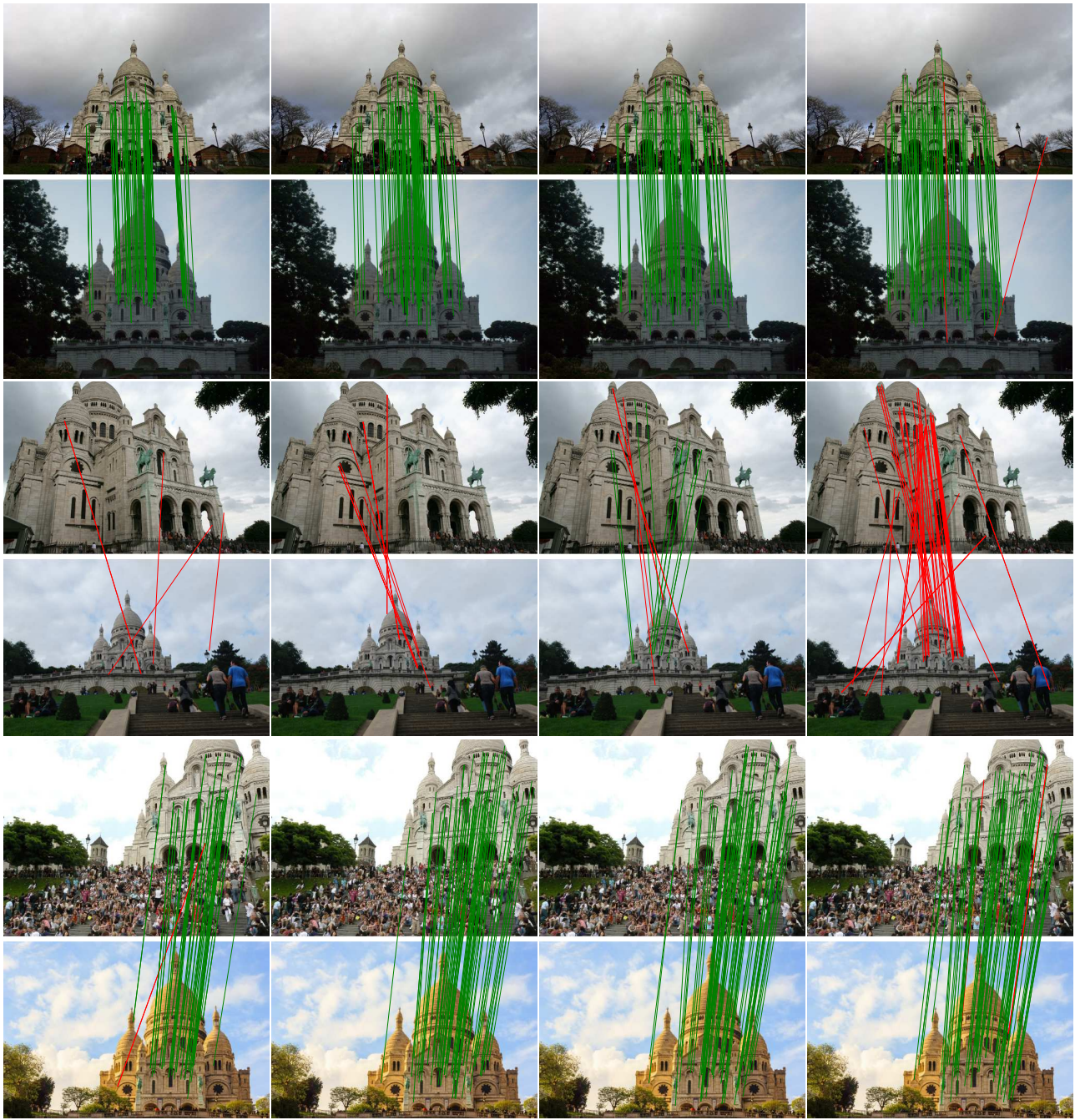
8.12. Outlier pre-filtering on the validation set

Due to space constraints, we do not include results on the validation set with CNe from the paper. We list them in Table 9, for SIFT with 8000 features, bidirectional matching with the ‘both’ strategy, and optimal ratio test thresholds. Without CNe we use optimal ratio test thresholds; with CNe we do not use the ratio test, as it was not trained for it and performs much worse in that case. Note that there are no parameters to set, which is why we report results directly on the test set in the main paper.

Additionally, we noticed one omission from the paper after the deadline: CNe was originally trained to estimate the Essential matrix instead of the Fundamental matrix [100], *i.e.*, assuming known intrinsics. In order to use it within our setup, we simply normalize by the size of the image instead of using ground truth calibration matrices.

8.13. Qualitative results

Fig. 24 shows qualitative results for stereo task – we draw the inliers produced by each method as in Fig. 1 in the main paper. The pair of images in the middle row have a very large baseline, and only HardNet is able to establish correct matches. Fig. 25 shows multiview results, displaying the importance of the detector, where D2-Net and AKAZE pick up more noise on the sky.



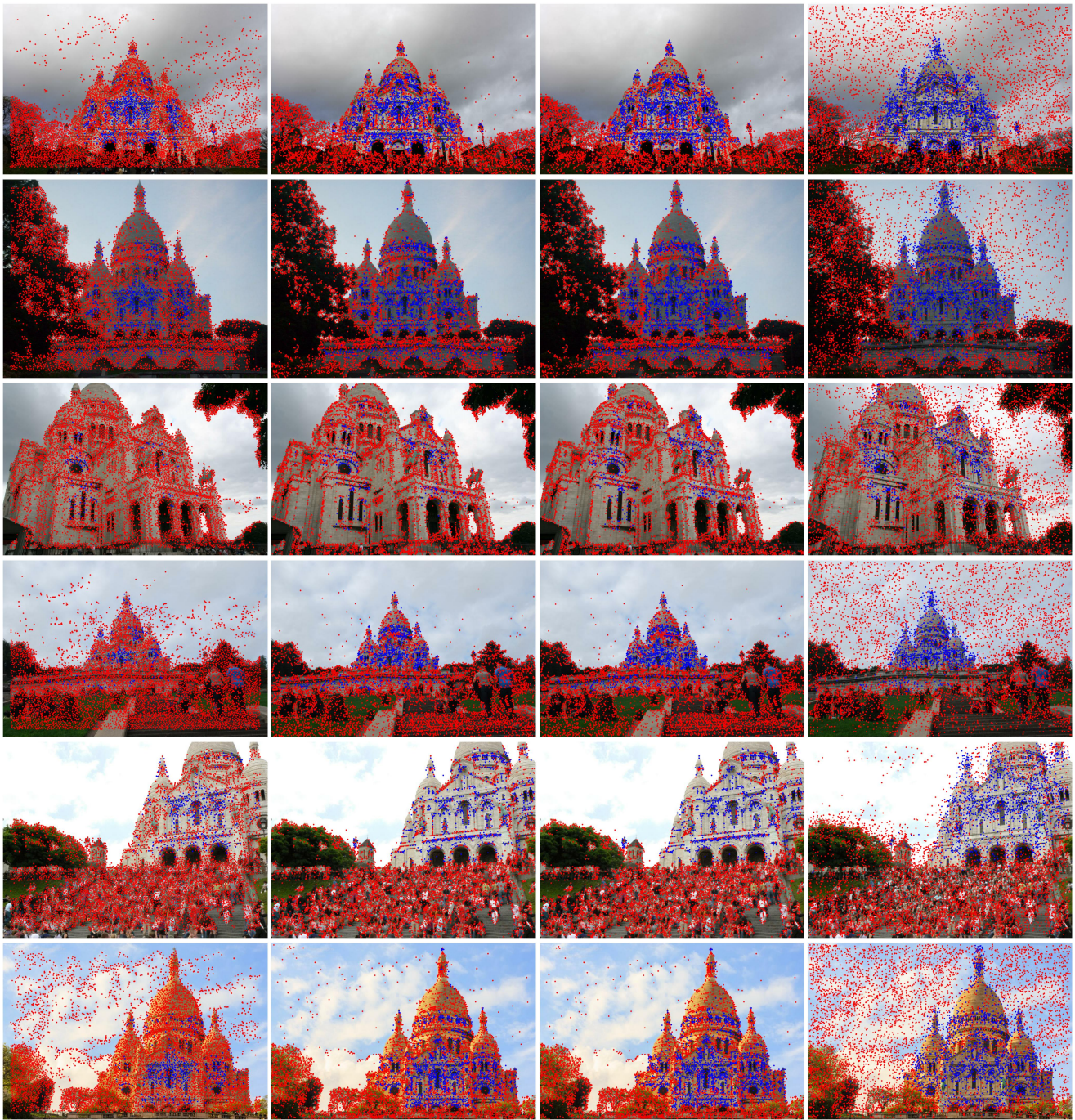
(a) AKAZE

(b) SIFT

(c) DoG+HardNet

(d) D2-Net

Figure 24. **Qualitative results for the stereo task** – Among the predicted matches using each method, we display the inliers in green, and the outliers in red.



(a) AKAZE

(b) SIFT

(c) DoG+HardNet

(d) D2-Net

Figure 25. **Qualitative results for the multi-view task** – We show images and detected keypoints for each method, with the 3D points identified by COLMAP in blue, and the ones that are not used in the 3D model as red. More blue points mean that more points are useful to reconstruct a 3D model. These results correspond to the ones where we use 25 images to reconstruct a 3D model.